PERGAMON

Journal of Structural Geology 21 (1999) 7–21

JOURNAL OF STRUCTURAL GEOLOGY

# Striated faults: visual appreciation of their constraint on possible paleostress tensors

Norman Fry [1]

*Laboratory for Strain Analysis, Department of Earth Sciences, Cardiff University, PO Box 914, Cardiff CF1 3YE, U.K.*

**Abstract**

Two new types of geometric representation provide visual appreciation of the extent to which a possible common stress tensor is constrained by a set of striated faults (solving the 'inverse problem'). The first type uses only orientation of fault plane and striation, and involves projections from a space, having dimensions of the six distinct elements of the stress tensor, in which faults are represented as poles on a hypersphere. Any girdle or clustering of poles permits identification of one or more normals, representing possible stress tensors. These tensors provide the dimensions of the second type of diagram in which directions represent both senses of shear and proportions in which component tensors are combined, so enabling identification of the total tensor which best matches the complete data. Examples illustrate uses for both homogeneous and heterogeneous sets of data, showing varying degrees of constraint on stress state. The discussion of mathematical issues includes the wider significance of tensor element space, regarding degrees of freedom, estimators of error and mismatch, and degeneracy. 

## 1. Introduction 1: stress tensor methods

This paper is offered as a contribution to those studies which, by integrating data from many striated faults, attempt to acquire information on past deviatoric stress. Other types of study integrate such data to attempt to obtain displacement patterns ('kinematics') or gross changes in shape of a rock-mass ('deformation' or 'strain'). The fundamental assumptions underlying studies of the type addressed here relate to stress only. They are as follows.

1. The stress tensor was constant through the space and time of generation of the fault set.
2. Each striation on a fault surface indicates the direction of the normal projection of the traction vector on that surface.

## 2. Introduction 2: visualisation of data sets

The importance of visual representation of constraints is well established in structural geology. One example is in the determination of a two-dimensional strain ratio from sets of elliptical markers. Algorithms exist for a direct calculation, such as that of summing second moments of ellipses (Shimamoto and Ikeda, 1976). However, the method is little used because it provides no information on the likely acceptability of the result, and in particular on the underlying assumption that the sample is representative of an isotropic population. Instead, structural geologists produce an $(R_f,\phi)$-plot (see, for example, Ramsay and Huber, 1983). Its representational space has orthogonal dimensions $R_f$ and $\phi$, neither of which correspond to dimensions of real space. Yet, it is the representation of choice for structural geologists. Visual matching of 'onion skins' may lack the simplistic quantifiable precision beloved of 'quality control', but it shows us the

[1] E-mail: FryN@cardiff.ac.uk

0191-8141/99 $ - see front matter 
PII: S0191-8141(98)00099-6

goodness of fit and the patchiness of our data, not just in summary but of how each individual datum sits within the set.

A second example relevant to this paper is the use of stereograms to show a great circle girdle of data points. The best fit circle and its goodness of fit may be calculated and presented non-graphically as summary quantities. Yet the stereogram remains worth plotting because it shows how each datum fits into and contributes to the pattern as a whole.

Studies of strain, fabric and fold analysis already enjoy visual appreciation of how data contribute to the overall estimation. The aim of this paper is to provide the same for studies of fault striation patterns.

## 3. Information used: essential and optional

The essential record of every fault consists of the attitude of the fault plane and the orientation of its striae. A record of sense of shear is not needed for every fault. A procedure which permits shear sense to be incorporated for only part of the data set is advantageous for three reasons:

1. Any striated fault constrains the range of possible stress tensors, even if its shear sense is unknown.
2. Interpreting field evidence of shear sense can be contentious, and is more prone to error than recording of orientations.
3. The mathematics of equalities is simpler than that of inequalities, leading to simpler graphical representation.

## 4. Conceptual basis of the main method: $\sigma$-space, f-poles and $\sigma$-vectors

Each datum consists of the direction cosines of two unit vectors: **n**, the fault normal and **b**, the direction in the fault plane at right angles to the striae. The assumption that the stress tensor, $\boldsymbol{\sigma}$, generates traction $(\boldsymbol{\sigma}.\mathbf{n})$ with zero component in the direction of **b** provides that $\mathbf{b}.(\boldsymbol{\sigma}.\mathbf{n}) = 0$. The latter equation has the expanded form

$$\sum_{i=1}^{i=3}\sum_{j=1}^{j=3} b_i\sigma_{ij}n_j = 0. \qquad (1)$$

This equation is linear in the six distinct elements of the symmetric matrix $\boldsymbol{\sigma}$, and it has known coefficients composed of $b_in_j$ products.

Equations of the above form in two or three variables have graphical representations which are well known. In two-dimensional $(x,y)$-space, an equation. $ax + by = 0$ represents a one-dimensional line through the origin to which the vector $\{a,b\}$ is perpendicular. In three-dimensional $(x,y,z)$-space, an equation $ax + by + cz = 0$ represents a two-dimensional plane through the origin with a normal vector $\{a,b,c\}$. These vector relationships are better displayed by rewriting in the forms: $\{a,b\}.\{x,y\} = 0$ and $\{a,b,c\}.\{x,y,z\} = 0$. Such equations specify the locus, which has one less dimension than the co-ordinate space, of all vectors perpendicular to the vector composed of the coefficients ($a,b$, etc.). They can be extended to any number of dimensions.

Eq. (1) represents in six-dimensional $\sigma$-element space (hereafter, '$\sigma$-space') a five-dimensional hyperplane with a vector normal given by its coefficients. Each fault datum provides the coefficients defining its own five-dimensional hyperplane. Any $\sigma$-space vector lying within that hyperplane represents a stress tensor capable of generating traction which accords with the fault datum. The problem of determining a common stress tensor is thus transformed into the geometric one of finding the common $\sigma$-space vector along which the hyperplanes representing the faults intersect. This is directly analogous to determining the intersections of planes in three dimensions. The latter would normally be considered in terms of great circles, which are the intersections of the planes with a surface of unit distance from the origin (a sphere). Their mutual point of intersection represents the planes' common linear direction. Similarly, hyperplanes in six dimensions will intersect a surface of unit distance from the origin (a 'hypersphere') along great hypercircles and their intersection will represent the common $\sigma$-space vector direction.

The practical problems of representing more than three dimensions can be alleviated in a number of ways. One is a careful choice of projection, which will be considered in the next section. Another is by using poles. Great circles are unwieldy, and great hypercircles unmanageable, but their poles can be represented as points in projections into two or three dimensions. To avoid ambiguity in what follows, a pole to the hyperplane representing a single fault in $\sigma$-space will be called an 'f-pole'. If the faults have a common generating stress, their f-poles will lie on a great hypercircle girdle (analogous to the great circle girdle of poles to planes with a common intersection in three-dimensions). The pole to this girdle represents the intersection direction of the hyperplanes. Its co-ordinates in $\sigma$-space are in proportions corresponding to the elements of the generating stress tensor. In vector terminology, the $\sigma$-space direction cosines of the vector normal to the girdle of f-poles, hereafter the '$\sigma$-vector', are in the proportions of the elements of the generating stress tensor.

## 5. Graphical concepts for projections out of more than three dimensions

Because the six $\sigma$-element dimensions of $\sigma$-space offer little subjective appreciation, there is no need for the co-ordinate axes of our plots to be restricted to them. For this paper, the six-dimensional array of f-poles is transformed to new orthogonal axes corresponding to the array's principal directions of second moment. Three of these new co-ordinate axes at a time are then selected for plotting f-poles co-ordinates, normally including the axis of fifth largest second moment, which is the initial candidate for the $\sigma$-vector of the array. (Explanation is given in Section 9.) However, this choice of co-ordinate axes and projection directions is not fundamental. Others may be found more suitable for extending the ideas proposed in this paper to new purposes or data sets.

The plots here are views of upper hemispheres, shown within a cage consisting of the basal circle and two vertical semicircles of intersection of the hemisphere with the principal planes. Because the three plotted co-ordinates do not sum to unity, the points lie within rather than on the surface of the hemisphere, as in Fig. 1. The selected co-ordinate axes of each plot are ordered, the forward, rightward and upward axes being of progressively smaller second moment. The reasons are as follows. If a girdle of f-poles exists, the moment towards its pole (the desired $\sigma$-vector) should be minimal. The digression of each f-pole away from a perfect girdle towards the candidate $\sigma$-vector is highlighted by having the girdle represented by the horizontal base and the $\sigma$-vector axis vertical, with each point joined to the base by a vertical line (Fig. 1a). If the f-poles do not extend around a girdle, but form a cluster, an entire plane of directions represents candidates for the desired $\sigma$-vector. The extent of such clustering is made more visible by having this plane of minimal moment lying vertically from left to right, leaving points concentrated in a back-to-front strip (Fig. 1b).

These projections retain maximum information content in several ways. Co-ordinates from $\sigma$-space are plotted the maximum number at a time (three in three-dimensional view). The co-ordinate values are not rescaled. So, each datum lies not on the hemisphere surface but inwards from it by an amount representing the root mean squared magnitude of its remaining (non-plotted) co-ordinates. It is represented not as a point but as the line (Fig. 1) from that point dropped along the direction of the least of the plotted moments perpendicularly onto the principal plane of higher moments. This helps to locate points, which otherwise appear to float ill-defined in three dimensions, as well as each line length representing the digression of that datum away from a hyperplane girdle.

## 6. Conceptual basis for incorporating recorded shear sense: q-space plots

The detailed handling of recorded shear sense varies, depending on the number of degrees of freedom left after analysis of the striation orientations. Each of the one or more acceptable $\sigma$-vectors is recomposed into its corresponding real-space stress tensor. Any sum or difference in any proportion of these tensors may be the stress condition appropriate for the data set. To constrain their proportions further, a graphical space is used, of which the contributing stress tensors are orthogonal axes. The co-ordinates of a point in this 'recorded shear sense quantifier'-space (hereafter 'q-space') are the weightings of these component stress tensors.

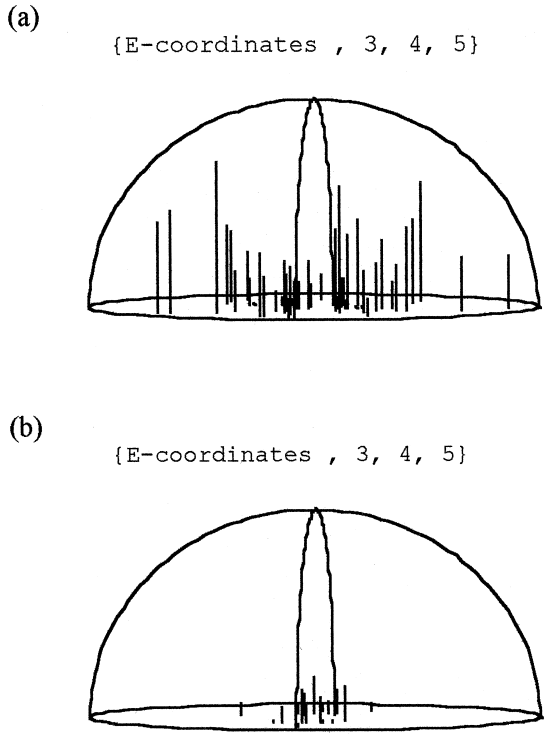


Fig. 1. Projections of f-poles using three $\sigma$-space co-ordinates at a time. (a) A data set inconsistent with assumption of a common stress tensor. The f-poles are at the apices of the vertical lines. Each line length represents the digression of the datum from the hypothetically best stress state girdle (the basal plane) towards its pole. The digressions are large for many of these data, indicating that these faults do not result from a single generating stress tensor. (b) A clustered data set. These data show a spread between the back and the front of the hemisphere only. Their very small spread along either the left-to-right or vertical axes indicates that they could have been generated by any stress tensor represented as any $\sigma$-vector in the left-to-right vertical plane.

The basis for this graphical technique is the calculation of 'recorded shear sense quantifiers' (hereafter 'quantifiers') for each fault for which a shear specification ('normal', 'sinistral', etc.) has been recorded. The quantifiers are positive if the computed and recorded senses agree, negative if they conflict (as detailed in Section 9). For each fault, evaluation of the quantifier for each of the candidate component stress tensors gives the respective axial component of a vector (**q**) in q-space. The ratio of these quantifiers is the ratio of their respective stress tensors in real space which would maximise the shear in the sense recorded for that fault. Any direction in q-space which is within a right angle of this vector represents proportions of component stress tensors which would produce the recorded sense.

The array of q-vector directions is compiled for the complete data set, giving a good visual appreciation of whether an overall stress tensor (direction in q-space) can be found which is consistent with (within a right angle in q-space of) most or all of the recorded shear senses. If such direction exists, its direction cosines are in the required proportions of the contributing component stress tensors.

In using this graphical procedure it is essential that the only component stress tensors used are those already known to be acceptable in terms of striation orientations. These q-space plots are conditional upon the result of, and not a substitute for, $\sigma$-space plots.

Table 1
Values used in the various stages of deriving a reduced stress tensor, as described in the text and illustrated in Fig. 2

| EXAMPLE OF A SIMPLE DATA SET | | | | | | | |
|---|---|---|---|---|---|---|---|
| Data presented to three decimal places but calculated to at least six significant figures. | | | | | | | |
| Raw Field Data (Fault plane orientation, striation direction, sense) | | | | | | | |
| Fault datum no. | 1 | 2 | 3 | 4 | 5 | 6 | 7 |
| Dip Azimuth | 283 | 110 | 089 | 147 | 045 | 360 | 050 |
| Dip | 86 | 35 | 32 | 36 | 47 | 90 | 66 |
| Bearing | 012 | 020 | 009 | 200 | 328 | 270 | 325 |
| Plunge | 18 | 06 | 07 | 15 | 13 | 08 | 12 |
| Sense | Dextral | Dextral | Dextral | Dextral | Sinistral | Dextral | Sinistral |
| Direction cosines (=axial vector components of unit vectors n and b) | | | | | | | |
| $n_1$ | −0.224 | 0.196 | −0.009 | 0.493 | −0.517 | −1.000 | −0.587 |
| $n_2$ | 0.972 | −0.539 | −0.530 | −0.320 | −0.517 | 0.000 | −0.700 |
| $n_3$ | 0.070 | 0.819 | 0.848 | 0.809 | 0.682 | 0.000 | 0.407 |
| $b_1$ | −0.287 | −0.280 | −0.189 | −0.125 | 0.241 | 0.000 | 0.080 |
| $b_2$ | −0.134 | 0.770 | 0.834 | 0.894 | 0.676 | −0.139 | 0.450 |
| $b_3$ | 0.948 | 0.574 | 0.519 | 0.430 | 0.696 | 0.990 | 0.890 |
| $\sigma$-space vector components of (non-unit) vector normal to hyperplane | | | | | | | |
| $b_1n_1$ | 0.064 | −0.055 | 0.002 | −0.062 | −0.125 | 0.000 | −0.047 |
| $b_2n_2$ | −0.131 | −0.415 | −0.442 | −0.286 | −0.350 | 0.000 | −0.315 |
| $b_3n_3$ | 0.066 | 0.470 | 0.440 | 0.348 | 0.475 | 0.000 | 0.362 |
| $b_1n_2 + b_2n_1$ | −0.249 | 0.302 | 0.092 | 0.481 | −0.475 | 0.139 | −0.320 |
| $b_2n_3 + b_3n_2$ | 0.913 | 0.321 | 0.432 | 0.586 | 0.101 | 0.000 | −0.440 |
| $b_3n_1 + b_1n_3$ | −0.233 | −0.117 | −0.165 | 0.111 | −0.195 | −0.990 | −0.490 |
| Magnitude of above $\sigma$-space vector composed from n,b coefficients | | | | | | | |
| | 0.987 | 0.777 | 0.782 | 0.891 | 0.798 | 1.000 | 0.876 |
| Vector components rescaled to unit magnitude (=f-pole co-ordinates) | | | | | | | |
| $p_1$ | 0.065 | −0.071 | 0.002 | −0.069 | −0.156 | 0.000 | −0.054 |
| $p_2$ | −0.132 | −0.534 | −0.565 | −0.321 | −0.438 | 0.000 | −0.359 |
| $p_3$ | 0.067 | 0.605 | 0.563 | 0.391 | 0.595 | 0.000 | 0.413 |
| $p_4$ | −0.252 | 0.389 | 0.118 | 0.540 | −0.595 | 0.139 | −0.365 |
| $p_5$ | 0.924 | 0.414 | 0.553 | 0.658 | 0.127 | 0.000 | −0.502 |
| $p_6$ | −0.236 | −0.151 | −0.211 | 0.124 | −0.245 | −0.990 | −0.559 |
| Magnitude of rescaled $\sigma$-space vector (as a check = unity) | | | | | | | |
| | 1.000 | 1.000 | 1.000 | 1.000 | 1.000 | 1.000 | 1.000 |
| New co-ordinates of f-poles (using principal second moment axes) | | | | | | | |
| $e_1$ | −0.684 | −0.927 | −0.992 | 0.772 | 0.663 | 0.298 | −0.261 |
| $e_2$ | 0.226 | 0.130 | 0.050 | −0.583 | 0.548 | 0.558 | −0.940 |
| $e_3$ | −0.231 | 0.040 | 0.058 | 0.031 | −0.420 | 0.769 | 0.145 |
| $e_4$ | 0.653 | −0.349 | −0.054 | 0.243 | −0.278 | 0.086 | −0.156 |
| $e_5$ | 0.027 | 0.001 | 0.079 | 0.056 | 0.082 | 0.036 | 0.045 |
| $e_6$ | 0.000 | 0.000 | 0.000 | 0.000 | 0.000 | 0.000 | 0.000 |
| Test of fault sense: calculated sense agrees with field record? | | | | | | | |
| | TRUE | TRUE | TRUE | TRUE | TRUE | FALSE | TRUE |

Table 2
Eigenvectors and eigenvalues of the second moment tensor derived from values in Table 1

| Ranking | Eigenvalue (scaled to 1st = 1.0) | Axial components in $\sigma$-space | | | | | |
|---|---|---|---|---|---|---|---|
| *6th* | *0.000* | *−0.57736* | *−0.57734* | *−0.57735* | *0.00000* | *0.00000* | *0.00000* |
| **5th** | **0.006** | **−0.80326** | **0.51371** | **0.28957** | **0.01411** | **0.07500** | **−0.03461** |
| 4th | 0.205 | −0.06788 | −0.19810 | 0.26598 | 0.77530 | −0.53276 | 0.02184 |
| 3rd | 0.241 | 0.10514 | 0.29513 | −0.40027 | 0.40806 | 0.24139 | −0.71892 |
| 2nd | 0.544 | −0.05320 | −0.13796 | 0.19116 | −0.47548 | −0.56425 | −0.63019 |
| 1st | 1.000 | −0.05419 | −0.50734 | 0.56153 | 0.07823 | 0.57783 | −0.29043 |

## 7. Some examples

### *7.1. A simple data set, with stress tensor well constrained in σ-space*

Seven striated fault data have been selected from a set of records of faults at Barry, near Cardiff, South Wales, UK. They are tabulated in the top section of Table 1. The stages in analysis of this set are detailed below.

Stage 1 is the conversion of field data into real space vector information in a standard form. In this example the required form is a set of direction cosines, using orthogonal axes (1,2,3) corresponding to (north, east, down), with the last always positive. These values, for the fault normal and the direction in the plane of the fault at right angles to the striation, being components of unit vectors **n** and **b**, respectively, are shown in the second section of Table 1.

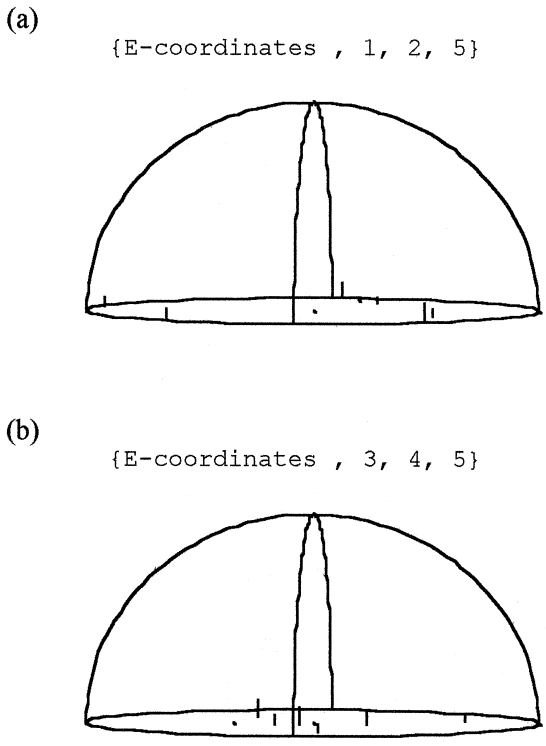


Fig. 2. A small data set permitting one possible stress tensor. The horizontal axes in (a) are the two directions of highest moments, in (b) those of intermediate moments. The low moment direction of the best $\sigma$-vector is vertical in both.

Stage 2 is the calculation of vector components in $\sigma$-space. The coefficients of each of the $\sigma_{ij}$ elements in Eq. (1) provide, for each fault, components of a vector which is normal to the hyperplane of acceptable stress states. However, the magnitude of this vector is not fixed. Division by its magnitude converts these components of the normal into six-dimensional direction cosines, which are the $\sigma$-space co-ordinates ($p$) of the f-poles. Both unscaled and scaled values are given in Table 1.

Stage 3 involves eigenvalues and eigenvectors of the second moment tensor of the array of f-poles. First, they have to be determined from the set of co-ordinates, $p$, and the results for this example are shown in Table 2. Then, they are used to calculate new co-ordinates ($e$) in $\sigma$-space, using as axes the eigenvectors in rank order of eigenvalue, as shown in the penultimate section of Table 1. Note that the sixth $e$ co-ordinate is systematically zero and is discarded (see Section 9). Within the remaining space, the direction which possesses least mean square f-pole component, hence lowest second moment, is the fifth $e$ co-ordinate axis. This is the best estimate of the $\sigma$-vector which represents a common generating stress tensor.

Stage 4 involves plotting and interpreting projections from $\sigma$-space using the new ($e$) co-ordinates. Fig. 2 shows two plots of values taken from Table 1, in both cases with the fifth co-ordinate vertical. These seven fault data show substantial spread within the basal planes of the plots (representing co-ordinate pairs 1,2 and 3,4, respectively), far more than of any datum up the vertical axis. That is to say, the top of the hemispheres in both parts of Fig. 2 really is the pole to a girdle of f-poles which spread through the other significant dimensions of $\sigma$-space. The vertical in Fig. 2 can be accepted as the direction of the desired $\sigma$-vector.

Stage 5 involves real-space tensors. The elements of the $\sigma$-vector from Table 2 are directly recomposed into

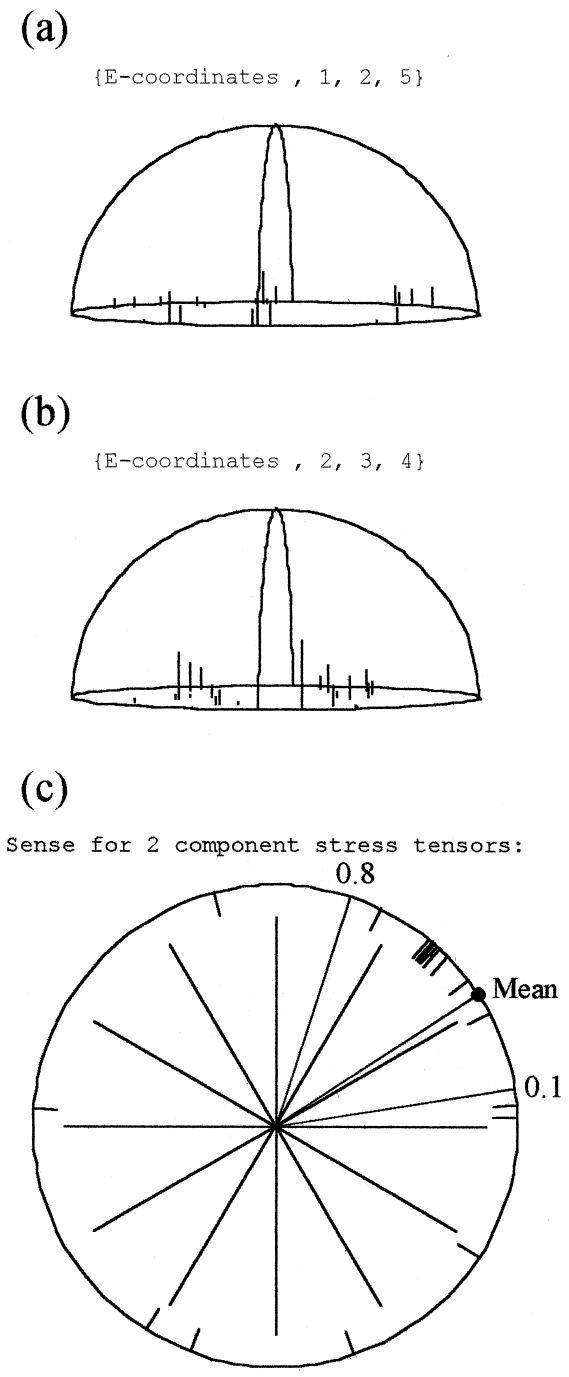


Fig. 3. Data, also illustrated in Fig. 1(b) for which a plane of possible $\sigma$-vectors exists. Here, the two principal moment directions within this plane are shown one at a time as vertical axes of (a) and (b). The use of these two $\sigma$-vectors leads to construction of the two-dimensional q-space plot (c). The large spot in (c) indicates the calculated mean direction (vector mean of unit vectors) in q-space. It can be seen that the recorded shear senses of three data conflict with this stress estimate, lying more than a right angle from its direction, while two more lie almost at right angles in q-space. These five data do not support the mean direction as a generating stress state. However, the relationship with the remainder of the data will be worsened if an alternative q-space vector is chosen which lies outside a restricted range around the mean. So, limits on compatibility with the remaining data, taken here to be $0.1(\pi/2)$ and $0.8(\pi/2)$ anticlockwise of the horizontal axis, are used to calculate a range of possible reduced stress tensor.

the stress tensor

$$\boldsymbol{\sigma} = \begin{bmatrix} -0.803 & 0.014 & -0.035 \\ 0.014 & 0.514 & 0.075 \\ -0.035 & 0.075 & 0.290 \end{bmatrix}.$$

However, the opposite pole in hyperspace is equally valid, and would give the negative of this tensor. The sense of motion of the calculated traction ($\boldsymbol{\sigma}.\mathbf{n}$) of each fault is now compared with that determined in the field. If the senses all agree, the stress tensor $\boldsymbol{\sigma}$ is used as it stands. If they all disagree, the negative of $\boldsymbol{\sigma}$ is used instead. The results of this test for this example are shown in the last section of Table 1. One fault sense contradicts, and either the field observation or the attribution of this datum to the common stress tensor is incorrect. Otherwise, the stress tensor has correct sign.

Stage 6 is the derivation from the stress tensor, $\boldsymbol{\sigma}$, of the orientations of its principal stress axes and of its stress ratio. This example gives, using tension positive convention, principal axes with bearing and plunge: $\sigma_1$ 359/02, $\sigma_2$ 263/73, $\sigma_3$ 090/17; and ratio of stress differences ('stress ratio') of $(\sigma_1-\sigma_2)/(\sigma_2-\sigma_3) = 4.0$.

### *7.2. Data sets consistent with more than one σ-vector, use of q-space*

#### *7.2.1. Two-dimensional q-space*

The data from which Fig. 1(b) was taken are displayed further in Fig. 3. The vertical axes in Fig. 3(a) and (b) are the directions of lowest and second lowest meaningful moments, respectively, (corresponding to the vertical and left-to-right axes of Fig. 1b). Although vertical co-ordinates in Fig. 3(b) are visibly greater than in Fig. 3(a), they are low in both cases and both axes are accepted for the purpose of this example as representing possible contributing tensors to the total tensor to be determined. Their two $\sigma$-vectors

$$\{0.579,\ -0.655,\ 0.076,\ 0.085,\ -0.347,\ 0.318\}$$
$$\{0.041,\ 0.472,\ -0.513,\ 0.322,\ -0.536,\ 0.348\}$$

are recomposed into real space stress tensors for the horizontal and vertical axes of a two-dimensional q-space plot (Fig. 3c). Using the direction cosines {0.837, 0.547} of the mean direction in Fig. 3(c) as the weighting coefficients for these two stress tensors gives the following initial estimate of total stress tensor;

$$\boldsymbol{\sigma} = \begin{bmatrix} 0.508 & 0.247 & 0.457 \\ 0.247 & -0.291 & -0.584 \\ 0.457 & -0.584 & -0.217 \end{bmatrix}.$$

Table 3
Best estimate of stress state derived from Fig. 3

| Tension positive | $0.1(\pi/2)$ | Mean | $0.8(\pi/2)$ | Compression positive |
|---|---|---|---|---|
| $\sigma_1$ axis | 356/27 | 357/27 | 250/21 | $\sigma_3$ axis |
| $\sigma_2$ axis | 233/47 | 246/35 | 353/30 | $\sigma_2$ axis |
| $\sigma_3$ axis | 104/30 | 115/43 | 129/52 | $\sigma_1$ axis |
| $(\sigma_1-\sigma_2)/(\sigma_2-\sigma_3)$ | 0.68 | 0.36 | 0.14 | $(\sigma_2-\sigma_3)/(\sigma_1-\sigma_2)$ |
| $(\sigma_2-\sigma_3)/(\sigma_1-\sigma_2)$ | 1.47 | 2.78 | 7.15 | $(\sigma_1-\sigma_2)/(\sigma_2-\sigma_3)$ |

Further consideration of (Fig. 3c) shows that, although five data are unable or unlikely to be consistent with the stress state responsible for the cluster of q-directions, a range of possible vectors can be accommodated by this cluster. Taking, for example, limits at $0.1(\pi/2)$ and at $0.8(\pi/2)$ anticlockwise of the horizontal axis, the corresponding direction cosines can be used to calculate reduced stress tensors, as above. Table 3 gives the stress orientations and differences derived from all the above three proportions of component tensors. Inspection of Table 3 shows that the directions of the principal stresses are well constrained, as is the identity of the axis of maximum compression. It also shows that the relative values of the other two principal stresses are ill constrained by this data set, and that there lies within this reasonable range of stress states a co-incidence of their values at which their possible identities interchange.

### 7.2.2. Three-dimensional q-space

Fig. 4 illustrates a set of faults for which there are three dimensions of very low co-ordinate values in $\sigma$-space. The three second moment eigenvectors which correspond to possible $\sigma$-vectors were calculated to be:

{0.615, 0.002, −0.617, 0.373, −0.316, −0.057}
{−0.410, 0.783, −0.373, 0.103, 0.100, −0.245}
{0.235, −0.194, −0.042, −0.096, 0.562, −0.762}.

Their corresponding real-space stress tensors are used as axes for a three-dimensional q-space diagram (Fig. 4c). This shows all shear sense data to be consistent with component proportions represented by the

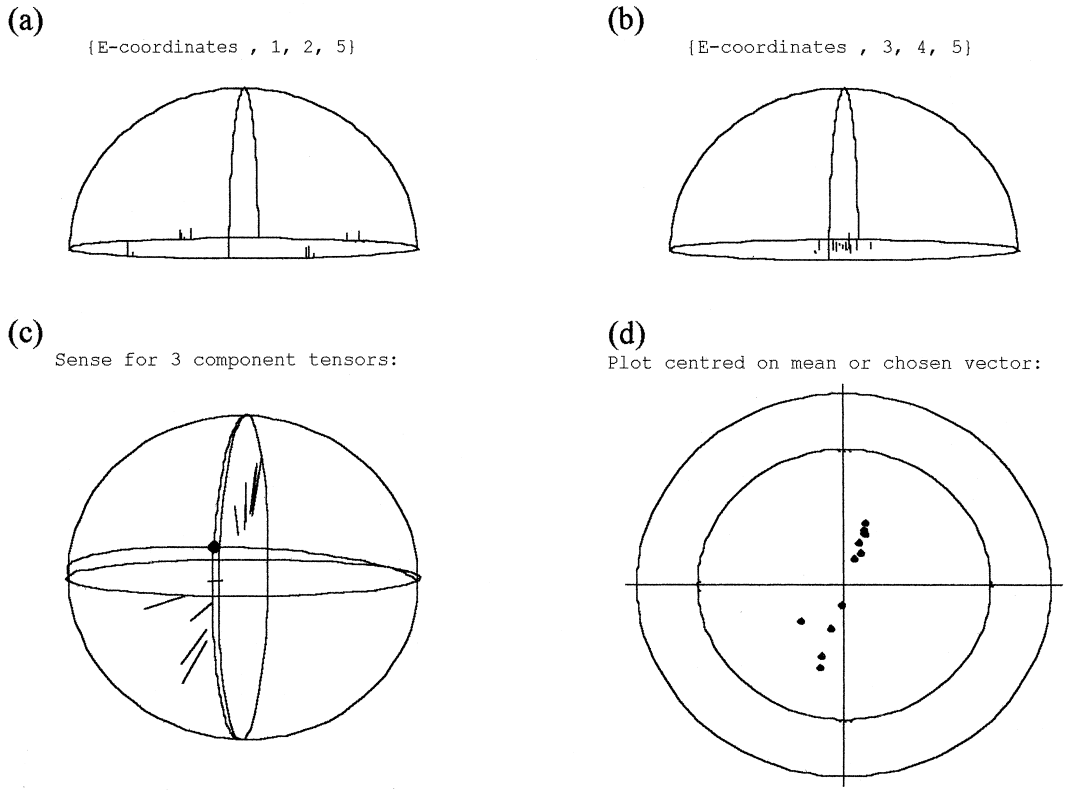


Fig. 4. The f-poles of this data lie almost on the plane of the greatest two moments, shown as the basal plane of (a). Their cluster extends very little toward any of the three axes of (b). All three of the latter are accepted as possible stress tensors. They are used for three-dimensional q-space analysis of shear sense (c), in which the radiating lines are the **q** vectors for the data, truncated to unit length at the spherical surface. The large spot at the intersection of two non-principal great circles indicates the mean direction (mean of unit vectors). Part (d) shows a plane projection of intersections with the sphere, centred at the mean. All data lie well within the inner circle representing a right angle from the mean. The mean lies centrally within the q-direction distribution. On these grounds the mean is accepted as a good estimate of total stress tensor, well consistent with all data.

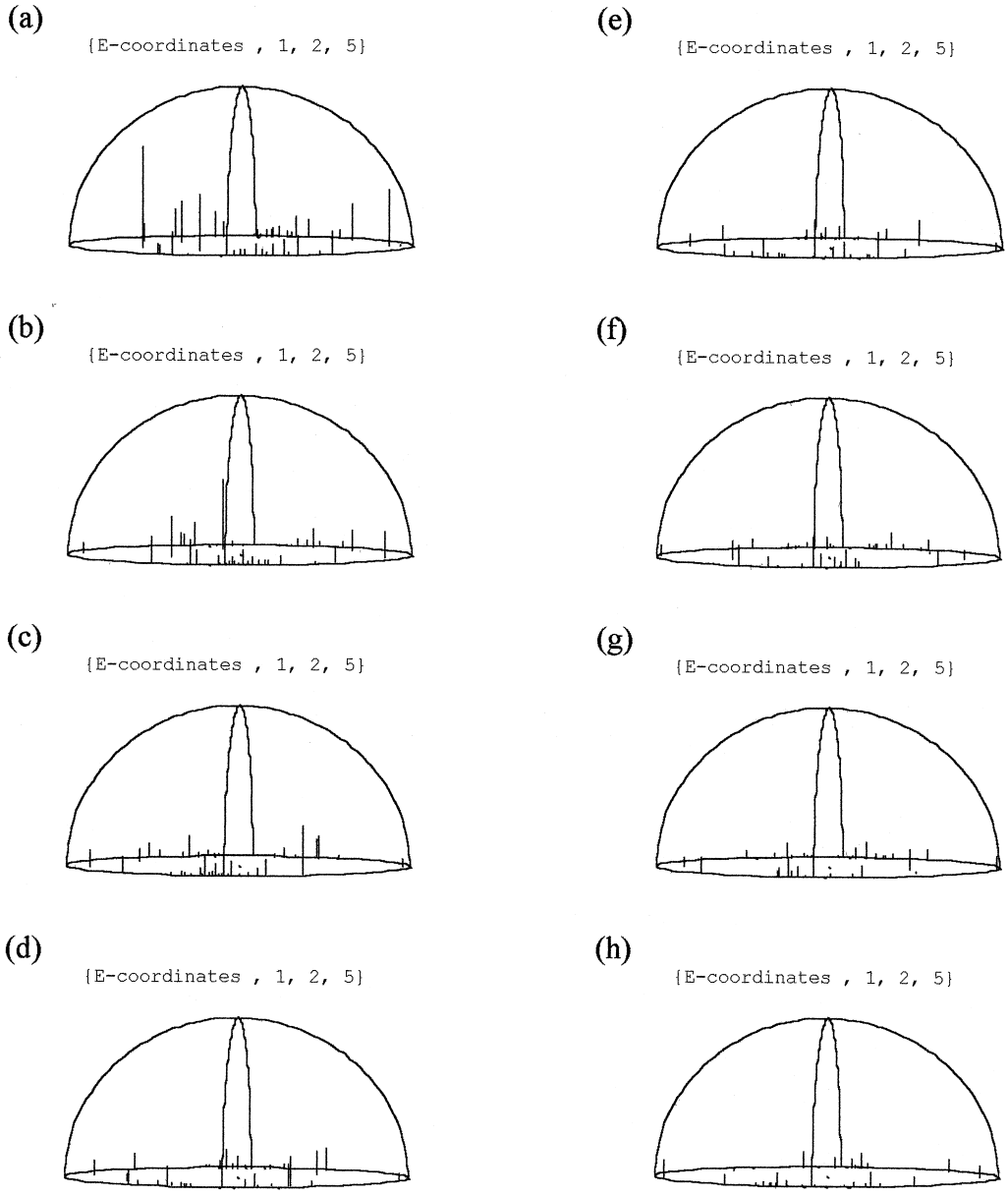


Fig. 5. Series of $\sigma$-space projections, each using the same moment axes, for an example of heterogeneous data. (a) The initial data include as identifiable subsets: (1) a trend of data rising from the backward–forward (maximum moment) axis around the surface of the right half of the hemisphere on a plane of about 25° tilt; (2) several scattered data of high vertical co-ordinate within the left half of the hemisphere. (b) Recalculated co-ordinates of remaining data after deletion of the furthest outlier in (a). (c)–(h) Each plot results from recalculation of moments and co-ordinates after deletion of the datum of highest vertical co-ordinate in the preceding plot. Changes are easily visible within the series (a)–(b)–(c)–(d), but not (d)–(e)–(f)–(g)–(h).

mean direction (Fig. 4d) with direction cosines {0.953, −0.033, 0.301}. On the basis of these coefficients, the reduced stress tensor (tension positive convention) has bearing and plunge of axial directions $\sigma_1$ 201/12, $\sigma_2$ 291/04, $\sigma_3$ 038/77, and stress ratio $(\sigma_1-\sigma_2)/(\sigma_2-\sigma_3) = 2.32$.

### 7.3. Heterogeneous data

In the previous examples, the distribution of f-poles in $\sigma$-space was such that they had very low co-ordinates in at least one dimension. They formed a girdle or cluster, for which one or more $\sigma$-vectors could be

identified and used to derive an estimate of the stress tensor. However, sets of fault data are often more problematic. They may combine data generated in one stress state with those generated in another, or contain spurious 'outliers'. The dangers of handling such data by regression are well discussed by Will and Powell (1991). A grid search alternative is appealing but has its own dangers. In particular, it is easy to mistake random clusters of data for meaningful signal, in the absence of some underlying appreciation of how data are distributed.

An example is presented here of a visibly heterogeneous set. The data in an initial $\sigma$-space projection (Fig. 5a) include, in the right half of the hemisphere, a trend not around the circumference of the basal plane (which in this projection represent proportions of the components of two greatest moments), but close to a plane rising up at about 25° to the right. Why do the summed second moments not have a principal plane through these data points, such that they plot around the basal circumference, as in the equivalent projections of Figs. 2–4? The reason is the large effect on second moments of those few data with high vertical co-ordinates in the left of the hemisphere. These are clearly outliers, not belonging to the girdle of data plotting to the right. The marked effect of deleting just the datum furthest to the top left is seen in Fig. 5(b). The recalculated co-ordinates now lie much closer to the basal circumference, but another outlier is now highlighted by a large vertical co-ordinate. The effects of deleting this, and then of the next point of high vertical co-ordinate, are seen in Fig. 5(c) and (d). It is clear in Fig. 5(d) that removal of just three outliers has resulted in the data lying in a girdle around the basal circumference of the plot.

For comparison, parts (e)–(h) of Fig. 5 show the effects on this same $\sigma$-space projection of a further four deletions, in each case of the point of greatest vertical co-ordinate in the preceding plot. The effect is almost negligible because the deleted data are close to the rest of the girdle. The associated stress parameters are shown in Table 4. Any of the subsets (d)–(h) may be taken as representative of the stress condition. Only when we could visually distinguish data outside the main girdle were we justified in expecting their deletion to improve the stress estimate. Once clearly misfitting data are removed, further removal of points may be a falsification rather than an improvement of the data.

Two further issues arising from this example will be given brief mention below, as they are deserving of further investigation.

### 7.4. Can a second stress tensor be estimated from a deleted subset?

It is useful to consider this matter as one of $\sigma$-space geometry. If the deleted data are consistent with a common stress, their f-poles lie on a second girdle. Two girdles on a hypersphere must have an area of intersection. In such a situation there almost inevitably must be data used to calculate the first stress estimate which belong to the second. More data than just the deleted points may be usable to estimate the second stress state. The optimum algorithm for allocating data to one subset or the other, or perhaps both with some appropriate weighting (despite their clearly not having simultaneously more than one generating stress state), is complex to the point of being beyond the scope of this paper.

### 7.5. Are stress tensors Andersonian?

The estimations of stress state after removal of two or more outliers (Table 4) all have principal stress axes within 10° of either horizontal or vertical. They approximate to the Andersonian condition of a vertical principal stress. The examples in Figs. 2 and 4 both have estimated axes within 17° of either horizontal or vertical. This appears to be no coincidence. Of the sets of data used to test the ideas in this paper, those which gave good definition of a $\sigma$-space vector have almost all produced an approximation to Andersonian conditions. One is led to speculate that only stress states with a vertical principal direction can be stably

Table 4
$\sigma$-vectors and corresponding real-space principal stress axes and strain ratios for progressive deletion of worst fitting data, as illustrated in Fig. 5. (Tension positive convention)

| Fig. 5 | $\sigma$-VECTOR | $\sigma_1$ axis | $\sigma_2$ axis | $\sigma_3$ axis | $(\sigma_1-\sigma_2)/(\sigma_2-\sigma_3)$ |
|---|---|---|---|---|---|
| (a) | {0.758, –0.587, –0.172, 0.218, –0.037, 0.056} | 099 06 | 252 84 | 009 03 | 0.473 |
| (b) | {0.752, –0.378, –0.374, 0.389, –0.022, 0.027} | 107 13 | 283 77 | 017 01 | 0.111 |
| (c) | {0.737, –0.344, –0.393, 0.420, –0.042, –0.078} | 108 09 | 312 80 | 199 04 | 0.073 |
| (d) | {0.742, –0.354, –0.388, 0.400, –0.044, –0.109} | 108 05 | 334 83 | 198 05 | 0.068 |
| (e) | {0.744, –0.355, –0.389, 0.386, –0.045, –0.138} | 107 01 | 011 83 | 198 07 | 0.056 |
| (f) | {0.746, –0.358, –0.389, 0.368, –0.044, –0.164} | 288 05 | 052 81 | 197 08 | 0.046 |
| (g) | {0.753, –0.362, –0.391, 0.351, –0.043, –0.152} | 286 01 | 024 83 | 196 07 | 0.042 |
| (h) | {0.767, –0.367, –0.400, 0.331, –0.027, –0.089} | 105 03 | 336 85 | 195 04 | 0.040 |

maintained throughout a large volume of rock and so give rise to data capable of determining a consistent stress tensor. Interestingly, on the basis of data used in this work, there does not seem to be any bias in favour of one particular regime within the Andersonian range. The examples in this paper were selected to illustrate plots, not for this purpose. Yet they happen to be varied. In the terminology of Fry (1992a), to which reference should be made regarding the propriety of earlier classificatory schemes, they are: Fig. 2: Extending Wrench; Fig. 4: Restricted Normal; Table 4: Contracting Wrench (close to Axial Contractional).

## 8. Summary plots of $\sigma$-space second moments

In addition to the projections of data from six dimensions, the main method of this paper provides values of the second moments of the f-pole array in their principal directions, which it is convenient to present in graphical form (Fig. 6). The form chosen here is a line graph, with straight sections between the values concerned, taken in order of decreasing moment. The display of gross differences between types of data set is convenient, when added to the other graphical methods described. However, to concentrate on summaries at the expense of plots of the full data would in general be contrary to the purpose of this paper.

## 9. Mathematical considerations

### *9.1. Degrees of freedom; stress tensor reduction*

The main mathematical procedure adopted here treats estimation of stress tensor as a problem in six variables in the first instance. This is unusual, as it is well known that two of the six degrees of freedom of the full stress tensor (absolute values of normal stresses, and an overall scale factor) cannot be constrained by striated fault data. All that can be estimated is a reduced stress tensor, related to the full tensor by

$$\boldsymbol{\sigma}_{\text{full}} = N\mathbf{I} + M\boldsymbol{\sigma}_{\text{reduced}}, \tag{2}$$

where $\mathbf{I}$ is the identity matrix and $N$ and $M$ are unknown scalars. Normal practice is to arbitrarily assign values, both for some measure of mean normal stress and for the scale of the reduced stress tensor, and then treat the problem as one in the four remaining variables.

The retention here of six variables is not only deliberate, it is fundamental to the search for a geometry suited to graphical representation. The two main handicaps in such a search are

1. unwillingness to abandon real-space dimensions for graphical representations; and
2. arbitrary assignment of values for unconstrained variables.

It does not matter how simple the geometry is in six dimensions, the geometry of the four-dimensional surface to which it is collapsed by addition of constraints may be either amenably simple or horrendously contorted, depending on the appropriateness of the applied constraints. The inappropriateness of arbitrarily assigned parameters is the essential reason why reduced stress tensors have been found so hard to represent graphically.

In the procedure adopted here, the two constraints of the stress tensor reduction are not arbitrarily assigned, but fall out naturally as the algorithm pro-

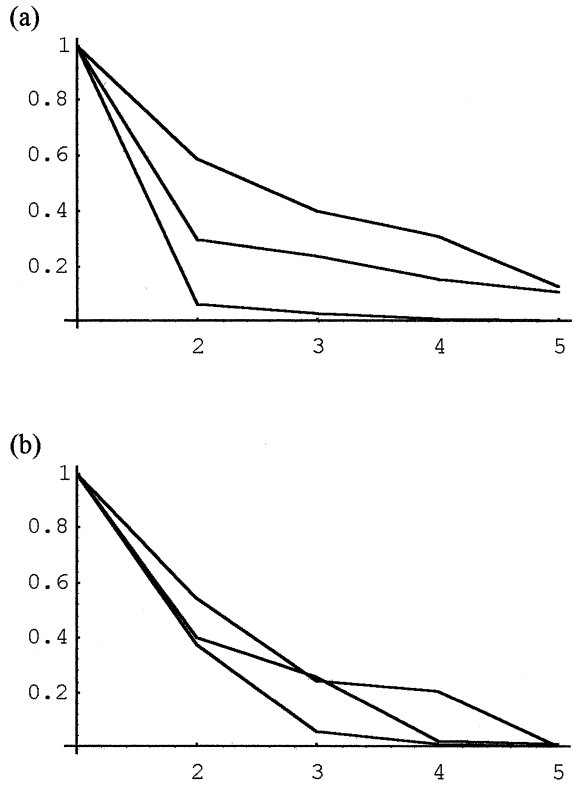


Fig. 6. Summary plots of principal second moment profiles for six data sets. Each profile is scaled to maximum moment of 1. (a) Three sets for which it is not reasonable to calculate a stress tensor. The highest and intermediate profiles are for data showing no concentration of f-poles into a girdle, indicating inconsistency of generating stress (the latter illustrated in Fig. 1a). The lowest profile has significant moment in only one dimension of $\sigma$-space. The 10 faults in this set hardly constrain stress tensor more than does a single fault, because all data give similar constraint. (See Sectopm 9.2) (b) Three data sets used in this paper as simple examples. That falling to zero only for the fifth calculated moment gives good constraint on stress tensor (Fig. 2). Those falling to near zero for two and for three moments, respectively, are those of Figs. 3 and 4, for which q-space plots were needed in the determination of stress tensor.

ceeds. It will be seen below that these correspond to restricting the $\sigma$-vectors representing stress states to lie on the intersection of a hyperplane with the unit hypersphere, thereby satisfying these equations.:

$$\sigma_{11} + \sigma_{22} + \sigma_{33} = 0 \tag{3}$$

$$\sigma_{11}^2 + \sigma_{22}^2 + \sigma_{33}^2 + \sigma_{12}^2 + \sigma_{23}^2 + \sigma_{31}^2 = 1. \tag{4}$$

The simplest possible reduction of dimensions is the distortionless reduction given by intersecting the space with a hyperplane represented algebraically by a linear equation such as (3). The geometric representation of scaling is the intersecting of all possible directions from the origin, representing unscaled proportions, by a closed surface. The simplest possible closed surface is the locus of points at unit distance from the origin (a hypersphere), as represented algebraically in Eq. (4). Thus, the four-dimensional surface of intersection of $\sigma$-space by one hyperplane and one hypersphere, as here, is the simplest possible geometry for represention of a reduced stress tensor. That is the fundamental strength of the main procedure of this paper.

Of the above restrictions for determining the reduction of stress tensor, that of Eq. (3) is commonly used (e.g. Angelier et al., 1982). The constant sum of squares of the distinct tensor components to give a unit $\sigma$-space hypersphere (Eq. 4) is novel.

It is quite possible to bow to the normal practice of reducing the numbers of variables at the start of the procedure, by collapsing the first three $\sigma$-space co-ordinates of each datum ($b_1n_1$,$b_2n_2$,$b_3n_3$) into two perpendicular co-ordinates on the plane defined by Eq. (3), and eventually reconverting the resulting first two direction cosines of a five-dimensional $\sigma'$-vector back into the three diagonal elements of the reduced stress tensor. However, the additional algorithmic complexity is not necessary.

### 9.2. Orthogonality of data

The most serious source of indeterminacy in fault striation analysis is a lack of spread of fault orientations.

Analogy with real space may be helpful on this point. Theoretically, we can determine from any two non-parallel directions the plane joining them. In practice, we know that the closer the lines are to being parallel, the more the similarity of the constraint which they put on the plane, and the less confidence we can have in the result. To obtain the best results, the lines should approach perpendicularity.

The problem of parallelism of data is considerably worse when trying to determine stress tensor from striated faults. In theory, only four faults are needed. For a good estimation, the relationship between them needs to be such that no pair is giving similar constraint. We can say that the data set should preferably approach 'orthogonality', not 'parallelism', but the meaning of such geometrical terms is, in the case of fault constraints, far from intuitively obvious. In fact, the space required to give these terms full meaning is the $\sigma$-space of this paper. The maximum constraint on stress tensor is achieved precisely when the four faults are represented by orthogonal f-pole vectors in $\sigma$-space. The determined $\sigma$-vector for the stress tensor is then truly orthogonal to all four data (as well as the isotropic stress $\sigma$-vector). A direct measure of orthogonality of any pair of faults is provided by the approach to zero of the dot product of their $\sigma$-space vectors.

### 9.3. Transformation to second moment axes and abandonment of sixth co-ordinate

In the six-dimensional $\sigma$-space used here, the hyperplane of possible $\sigma$-vectors for any fault is given by Eq. (1), which in expanded form is

$$b_1n_1\sigma_{11} + b_2n_2\sigma_{22} + b_3n_3\sigma_{33} + (b_1n_2 + b_2n_1)\sigma_{12} + (b_2n_3 + b_3n_2)\sigma_{23} + (b_3n_1 + b_1n_3)\sigma_{31} = 0. \tag{5}$$

However, because the **n** and **b** vectors are perpendicular in real space, the first three coefficients always sum to zero:

$$b_1n_1 + b_2n_2 + b_3n_3 = \mathbf{b}.\mathbf{n} = 0. \tag{6}$$

Therefore, any $\sigma$-space vector of the form $\{a,a,a,0,0,0\}$ satisfies Eq. (5). If a set of faults constrains the reduced stress tensor perfectly, the set of corresponding hyperplanes in $\sigma$-space intersect in the entire plane containing both the $\sigma$-vector representation of that reduced tensor and $\{a,a,a,0,0,0\}$. This plane is the geometrical representation in $\sigma$-space of any sum of the reduced stress tensor to be evaluated plus an isotropic normal stress ($N\mathbf{I}$ in Eq. 2), in any proportion.

The procedure for transformation to new axes is one commonly used for determining multivariate principal variation vectors, only in this case it is the directions of least variation which are of particular interest. First, a $6 \times 6$ matrix is created for each datum. This matrix is the outer product of the f-pole vector with itself. That is to say, if **p** is the unit vector of the f-pole, giving the direction of non-unit vector $\{b_1n_1, b_2n_2, b_3n_3, (b_1n_2 + b_2n_1),(b_2n_3 + b_3n_2),(b_3n_1 + b_1n_3)\}$, element $i,j$ of the matrix has value $(p_i.p_j)$. The sum of these matrices over all faults is that of the second moment (Scheidegger) tensor of the array. Its eigenvalues are the second moments of the array in the principal directions given by its eigenvectors. The matrix needed to perform the transformation of co-ordinates from initial axes to these principal axes is

composed of the eigenvectors. (See any book covering eigenvector analysis, such as the 'Introduction' and 'Jacobi Transformations' sections of the chapter 'Eigensystems' in Press et al., 1992.)

In practice, the effect of this procedure is that the isotropic stress $\sigma$-space eigenvector $\pm\{(1/3)^{1/2},(1/3)^{1/2},(1/3)^{1/2},0,0,0\}$ is that of minimum (sixth largest) eigenvalue, while even a perfect set of faults recorded in the field will give a reduced stress $\sigma$-vector as the eigenvector of second least (fifth largest) eigenvalue. The reason for this is that although both eigenvalues are theoretically zero, they differ by several orders of magnitude in their precision. That of the isotropic stress eigenvalue results from machine precision, whereas that of the reduced stress eigenvalue results from the precision of the field records of fault orientations. Table 2 provides an example where the difference in precision is between four and five orders of magnitude, such that the first three elements of the eigenvector of sixth eigenvalue differ only in their fifth decimal places from $(1/3)^{1/2} = 0.577350$. Consequently, in the procedure here, the sixth eigenvector is simply discarded together with all the co-ordinates of the f-poles along its axis (all zero, as in Table 2). The remaining five new co-ordinate axes are those of the reduced $\sigma$-space which it is meaningful to represent graphically and in which to search for suitable $\sigma$-vector of a reduced stress tensor. That is why the fifth eigenvalue axis is that plotted vertically in most projections from $\sigma$-space, and only five values are shown on the summary plots of $\sigma$-space second moments (Fig. 6).

An exception to the above observations will occur if the procedure is used on a set of model data which have been calculated to machine precision. For such a set, the orthogonal fifth and sixth eigenvectors will lie in the correct plane, but rotated from the two vectors required. In such a case, the fifth eigenvector and the stress tensor recomposed from it will not be reduced to the condition given by Eq. (3). However, the principal stress orientations and stress ratios calculated from it will still be correct.

### 9.4. Acceptability and indeterminacy

In any procedure to solve 'the inverse problem' (resolving $\boldsymbol{\sigma}$ back from partial information about its consequences), it is necessary to consider how much misfit between recorded and computed values is acceptable. Sometimes, residual misfit is specified in terms of field measurements. The implication behind such a formulation is that stress tensors are unvarying across the space and time of generation of the faults being considered, and that errors are due to human failings. This conceptual attitude is not justified. It is more than possible that the main digressions from a simple determination are due to real changes in stress tensor. Indeed, it is not unreasonable to doubt whether a stress state will ever be maintained across sufficient time and space to produce a fault set ideally suited to fault striation methods. We are in the business of testing the reasonableness of an approximation, in this case of approximation to a common reduced stress tensor.

Additional problems arise when limits to field observations are given in absolute terms:

As discussed elsewhere (Fry, 1992b), the field parameters for recording planes are not independent and vary in their determinacy. To take just one example, if a plane dips at three degrees, an angular error of, say, 30° in recorded strike or dip-azimuth is of no consequence. The resulting error in its fault-normal $\mathbf{n}$ is less than for a plane dipping at 45° with 3° errors in each measurement. As dip tends to zero, strike or dip-azimuth become completely indeterminate. Any specification of limit in absolute terms is inappropriate.

Absolute limit of striation orientation (e.g. Hardcastle and Hills, 1991) is even more problematic. Setting aside both problems associated with different methods of measuring linear directions in the field and problems analogous to those for planes, discussed above, there can be relative orientations of fault plane and stress tensor at which small changes in stress cause large changes of striation direction. Worse still, occurrence of such relative orientations can only be known in hindsight, after the stress determination is complete. However, in practical terms, this should be of no consequence. If large variations in striation direction correspond to small changes of stress tensor, larger than normal errors in striation will affect the determined stress tensor negligibly. Again, an absolute limit in terms of field measurement is not appropriate.

To avoid the kinds of problems mentioned above, limits to acceptability of data need to be set, and calculations of residual errors undertaken, in a way which is

1. consistent,
2. reasonable for handling variability of stress tensor as well as measurement error, and
3. proportionate in its effects on the determined stress tensor.

The $\sigma$-space geometry of this paper provides the framework required, giving an improvement on the formulation in Fry (1992b). As discussed in that paper, angular fitting errors can be best estimated by the divergences between vectors. These may be evaluated in $\sigma$-space as simply unity minus the dot product of unit vectors $\left(1 - \sum_{i=1}^{i=6} u_i v_i.\text{ for unit vectors } \mathbf{u}, \mathbf{v}\right)$, whether the vectors concerned represent faults (as f-poles), stress tensors, or a relationship of one to

Table 5
Recorded shear sense quantifiers ($q_i$) for q-space vectors

| Sense | Quantifier $q(\mathbf{r},\mathbf{n})$ | Alternatives | Quantifier $q(n,\sigma$ elements) |
|---|---|---|---|
| Normal | $r_1.n_1 + r_2.n_2$ | $-r_3.n_3$ | $n_3\Sigma_{i=1}^{i=3} n_i(\sigma_{i3} - n_3\Sigma_{j=1}^{j=3}\sigma_{ij}n_j)$ |
| Reverse | $-(r_1.n_1 + r_2.n_2)$ | $r_3.n_3$ | $-n_3\Sigma_{i=1}^{i=3} n_i(\sigma_{i3} - n_3\Sigma_{j=1}^{j=3}\sigma_{ij}n_j)$ |
| Sinistral | $r_1.n_2 - r_2.n_1$ | $(t_1.n_2 - t_2.n_1)$ | $\Sigma_{j=1}^{j=3}(n_2\sigma_{1j}n_j - n_1\sigma_{2j}n_j)$ |
| Dextral | $r_2.n_1 - r_1.n_2$ | $-(r_1.n_2 - r_2.n_1) = -(t_1.n_2 - t_2.n_1)$ | $-\Sigma_{j=1}^{j=3}(n_2\sigma_{1j}n_j - n_1\sigma_{2j}n_j)$ |
| None | 0 | 0 | 0 |

another. (See discussion of angular misfit in Fry, 1992b.)

### 9.5. Vector relationships in q-space

The 'recorded shear sense quantifiers', for faults for which shear specifications have been recorded, are formulated in Table 5. Real-space vector **r** is the resolved traction (sometimes referred to as 'resolved shear stress') in the plane of the fault, given using the star product of De Paor (1990) and in traditional form by

$$\mathbf{r} = \mathbf{t} - \mathbf{n} * \mathbf{t} = \mathbf{t} - (\mathbf{t}.\mathbf{n})\mathbf{n}. \quad (7)$$

Each quantifier is a scalar, defined here as a function of **r** and **n**. The final column gives forms suitable for programming in languages unable to handle vector algebra, but in so doing it also illustrates an important attribute of the these quantifiers. Like **r** and **t**, through which they are derived, they are all linear in elements of $\sigma$.

On account of the linearity in elements of $\boldsymbol{\sigma}$, the following will apply for each fault with specified shear sense. A linear combination of possible component stress tensors will produce a proportionate linear combination of their respective quantifiers. That is, if a total stress tensor has component tensors $\boldsymbol{\sigma}_i$ (the subscript after bold $\boldsymbol{\sigma}$ denoting each of several tensors, not elements) for which the calculated quantifiers are $q_i$, then $\boldsymbol{\sigma}_{\text{total}} = \Sigma x_i\boldsymbol{\sigma}$ and $q_{\text{total}} = \Sigma x_i q_i$, where $x_i$ denotes the amount of each contributing component tensor. In q-space, these amounts ($x_i$) are co-ordinates along respective ($i$) axes. The total quantifier $\Sigma q_i x_i$ is the dot product (**q.x**) of the q-space vector **x**, giving the amounts of the component tensors, with a q-space vector $\mathbf{q} = \{q_1, q_2, \ldots\}$, giving the magnitudes of their quantifiers. The plane $\Sigma q_i x_i = 0$ is the locus of combinations of tensor components resulting in no computed shear on the fault. It separates the half-space $\Sigma q_i x_i > 0$, in which computed shear sense accords with that recorded, from the half-space $\Sigma q_i x_i < 0$, in which computed and recorded sense conflict. The normal to this plane is the (non-unit) vector **q**. Its direction represents the fault in q-space.

If a q-space vector **x** can be found which is within a right angle of the **q** vector of every fault, the total stress tensor which **x** represents would in all cases produce shear in the sense recorded. If suitable **x** exists, its co-ordinates are the coefficients for summing the component tensors derived from $\sigma$-space vectors to the appropriate total reduced stress tensor.

In the case of only one $\sigma$-vector consistent with the data, the above procedure reduces to calculating the sign of the recorded shear sense quantifier for each fault. The appropriate reduced stress tensor may be the one directly recomposed from the $\sigma$-vector, or its negative. If the sum of the quantifiers is negative, the signs of the reduced stress tensor and all quantifiers are reversed, and a non-visual assessment made of the how many and which faults have recorded sense inconsistent with the majority. (It is convenient to program automatic testing and reversal of signs for stress tensors, including when more than one is acceptable, because the majority of faults will then plot in the positive quadrant or octant in q-space.)

The restriction emphasised above, that the dimensions of q-space must be only those of component stress tensors acceptable in terms of $\sigma$-space vectors, is essential. The q-space procedure only calculates the relative magnitudes of shear in the direction of the striae on the assumption that the striation direction is correct. If it is not, there may be other components of shear oblique to the striae as recorded, in which case the bounding plane in q-space represents not minimal shear but a likelihood that resultant shear will be in a direction other than that accepted as correct for the rest of the q-space plot. In other words, the preconditions for the q-space method would be violated.

### 9.6. Real space axes and conventions

The choice of axes for describing orientations in real space does not affect the $\sigma$-space procedures, although the processing of the resulting recomposed real-space stress tensor(s) must accord with the axes adopted for input of the **n** and **b** data. However, the q-space procedures are convention dependent. Simpler quantifiers than those in Table 5 are possible, some in terms of **r** or **t** alone, if conventions are always strictly adhered to regarding the signs of components of both **n** and $\boldsymbol{\sigma}$, corresponding to restricting the fault wall under con-

sideration to particular hemispheres. In practice, it is more complex to test and correct for such conventions than to use the quantifiers shown. The forms in Table 5, by relying on correspondences between **r** (or **t**) and **n**, allow such conventions to be relaxed, leaving only the following. Denoting the co-ordinate axes associated with subscripts 1,2,3 as $x,y,z$, the quantifiers tabulated in Table 5 assume that

1. polarity of vectors and axes are consistent, so that positive $x,y,z$, for **t** correspond to positive $x,y,z$, for **n**;
2. $z$ is vertical;
3. tension is positive;
4. positive $y$ is clockwise from positive $x$ when viewed from above.

Violation of assumption (1), for example by trying to adhere concurrently both to the general non-geological convention that **n** is away from the fault plane and the peculiarly geological convention of positive compression, is likely to be troublesome, and can only be made good by very careful re-evaluation of the signs of traction vectors of types 'normal', 'reverse', 'sinistral' and 'dextral' for the alternative conventions adopted. Assuming that conventions (1) and (2) above are adhered to:

1. Use of stress tensor with a compression positive convention requires only interchange of the normal and reverse quantifiers.
2. Use of positive $y$ anticlockwise from positive $x$ requires only interchange of the sinistral and dextral quantifiers.
3. If $z$ is not taken as vertical, analogous conventions can be deduced by appropriate substitutions of the axial subscripts in Table 5.

## 10. Conclusions

The methods introduced in this paper have wide potential application to the study of striated faults.

1. The visualisations of $\sigma$-space and q-space diagrams provide insight into the validity of existing estimates of reduced stress tensor.
2. The visualisations may indicate that it is more reasonable to deduce a range of possible stress states, as in the example of Fig. 3, rather than a single best estimate.
3. These methods allow a complete set of striated faults, only a proportion of which have clear movement sense, to be incorporated into a single procedure for testing homogeneity.
4. These methods can provide a complete reduced paleostress determination, as set out for the example in Fig. 2.

Perhaps the greatest benefit of these procedures would be if increased appreciation of data helped to overcome the present impasse. On the one hand there are those with unshakeable faith in paleostress determinations from fault striations. On the other, there are those who realise the particularity of the conditions required for even a limited number of faults to record the same stress state, and who consequently reject all such evidence. These graphical illustrations and visual appreciation, of how good or poor such data really are, may be able to bring the two parties to an eventual accommodation.

## Acknowledgements

This work has benefitted from discussions with colleagues of the Laboratory for Strain Analysis, Cardiff. Rodney Gayer, Richard Lisle and Michal Nemcok provided data used in development; Mike O'Hara gave assistance with computing and general encouragement. Above all, Sara Vandycke's appreciation of the subject was inspirational, particularly her understanding that it is not just foolish but theoretically impossible to associate a fault with a stress regime at the time of recording. Her statement "One fault permits many varied stress regimes; many varied faults permit one regime." is in this paper translated into a geometric relationship. The hyperplane of stress states consistent with a fault has dimensions only one less than the space of all stress tensors; fault poles must spread through all other dimensions in order to limit to one remaining dimension the permitted stress state.

## References

Angelier, J., Tarantola, A., Valette, B., Manoussis, S., 1982. Inversion of field data in fault tectonics to obtain the regional stress—1. Single phase fault populations: a new method of computing the stress tensor. Geophysical Journal of the Royal Astronomical Society 69, 607–621.

De Paor, D.G., 1990. The theory of shear stress and shear strain on planes inclined to the principal directions. Journal of Structural Geology 12, 923–927.

Fry, N., 1992a. Stress ratio determinations from striated faults: a spherical plot for cases of near-vertical principal stress. Journal of Structural Geology 14, 1121–1131.

Fry, N., 1992b. A robust approach to the calculation of paleostress fields from fault plane data: Discussion. Journal of Structural Geology 14, 635–637.

Hardcastle, K.C., Hills, L.S., 1991. BRUTE3 and SELECT: Quickbasic 4 programs for determination of stress tensor configurations and separation of heterogeneous populations of fault-slip data. Computing Geoscience 17, 23–43.

Press, W.H., Flannery, B.P., Teukolsky, S.A., Vetterling, W.T., 1992. Numerical Recipes: the Art of Scientific Computing. 2nd edn. Cambridge University Press.

Ramsay, J.G., Huber, M.I., 1983. The techniques of modern structural geology, 1. Academic Press.

Shimamoto, T., Ikeda, Y., 1976. A simple algebraic method for strain determination from deformed elliptical objects.—I. Basic theory. Tectonophysics 36, 315–337.

Will, T.M., Powell, R., 1991. A robust approach to the calculation of paleostress fields from fault plane data. Journal of Structural Geology 13, 813–821.